The International Journal of Advanced Manufacturing Technology (2023) 127:2343–2355
https://doi.org/10.1007/s00170-023-11612-w

ORIGINAL ARTICLE

Metal matrix composite fabricated from electrospun PAN, EGNS/PAN nanofibers and AL 5049 alloy by using friction stir processing

Saleh S. Abdelhady[1] · Rehab E. Elbadawi[2] · Said H. Zoalfakar[1]

Received: 26 February 2023 / Accepted: 19 May 2023 / Published online: 3 June 2023

Abstract
This work is an attempt to fabricate aluminum (AA 5049) matrix composites (AMCs) reinforced with electrospun polyacrylonitrile (PAN) nanofibers and consisting of exfoliated graphite nanosheets (EGNS/PAN) by utilizing friction stir processing (FSP) to improve the mechanical characteristics of AA 5049. The electrospinning method was used for fabricating PAN and EGNS/PAN nanofibers. The average diameter of the electrospun PAN nanofibers is 195 ± 57 nm, and after EGNS incorporation is 180 ± 68 nm. Dynamic recrystallization was the main process in the microstructure evolution of the stir zone during the FSP with PAN and EGNS/PAN nanofibers. According to PAN and EGNS/PAN nanofibers were used in the FSP procedure, the grain size reduced as a result of the pinning effects. PAN and EGNS/PAN nanofiber reinforcement enhanced the hardness to 89 and 98 Hv, respectively. Also, the ultimate tensile strength was raised to 291 MPa and 344 MPa, respectively. Tensile strength and hardness of the stir zone increased during the FSP with PAN and EGNS/PAN nanofibers due to the higher density of the strengthening mechanisms of grain boundaries and dislocations. The mechanical characteristics of AA5049 can be enhanced by the procedure of incorporating nanofibers, making them an ideal choice for applications in the automotive and aerospace industries.

Keywords Metal matrix composites · Electrospinning · Nanofibers · Aluminum · Friction stir process · Mechanical properties

1 Introduction

Ceramic and carbon nanofibers were utilized as the reinforcing fibers for metal matrices such aluminum and magnesium. Using ceramic nanofibers as a reinforcement to improve the mechanical characteristics of metal matrix composites [1, 2]. However, the percentage of reinforcement needs to be optimized to improve the mechanical properties (such strength, hardness, and Young's modulus) of the composites [3].

A promising method called electrospinning enables the creation of micro or nanofibers with the potential to form membranes with linked porosity, superior mechanical characteristics, and a large surface area. The technology of electrospinning has numerous applications, including in the fields of medicine [4], energy transportation [5, 6], optoelectronic devices [7, 8], and water treatment [9–13]. Micro- and nanoscale electrospinning can be used to create electrospun fibers with the potential to incorporate cutting-edge materials to enhance their mechanical or physicochemical properties [14–16]. Continuous and non-woven fibers with micro and nanoscale dimensions can be created using the electrospinning technique [17, 18]. The electrospun fibers were therefore excellent for potential applications in a wide range of fields, including the conveyance of energy [19], membrane [20, 21], adsorption processes [22], and air filtration [23, 24], Among the topics covered are medication delivery [25, 26], plat grafting [27], optoelectronic devices [28, 29], electrochemical sensors [30], and others. The electrospinning process is defined as the point at which the polymer solution and electric field interact. The voltage applied causes uncompensated charges to accumulate on the polymeric surface. The forces caused the polymer chains to align as they passed through the needle shear. This phenomenon produces a jet and Taylor's

✉ Saleh S. Abdelhady
salehgaballa@hotmail.com

[1] Department of Mechanical Engineering, Higher Technological Institute, P.O. Box: 228, 10th of Ramadan City, Egypt

[2] Department of Mechanical Engineering, Mechatronics Engineering Program, Egyptian Academy for Engineering and Advanced Technology (EAEAT), Cairo City, Egypt

cone, a conical shape over the solution. A linear jet that leaves Taylor's cone accelerates towards the collector. The intermolecular stability of the polymer is then maintained as the solvent evaporates while the jet is in motion. The fibers are then gathered and spread throughout the collector surface to create a non-woven mesh [13, 31, 32].

The manufacturing of aluminum matrix composites (AMCs) has recently become more significant due to applications in sectors including aerospace and automotive. This is because they have a number of prospective advantages over conventional alloys, such as great formability, improved wear resistance, higher specific stiffness, favorable fatigue properties, and outstanding strength to weight ratio at low or high temperatures [33].

On the other hand, there are several surface modification processes, including the laser melt technique, centrifugal casting, and plasma spraying, which are used to modify only the surface of a material while leaving the interior unaltered. When using such methods, the bulk of the material loses a tiny number of other attributes like toughness while surface properties like hardness and wear resistance only slightly improve [34]. While all these techniques have been utilized effectively to make surface MMCs, a major concern is that they need material phase transitions throughout the process (from solid to liquid or from liquid to vapor). As a result of the interfacial interactions between the material and the reinforcement caused by the phase change, the interfacial bonding strength is reduced, and harmful phases are formed [35].

A possible solid-state processing method for creating surface MMCs and customizing the surface's microstructure through extreme plastic deformation is friction stir processing (FSP) [36–38]. When compared to alternative methods, FSP is quicker, uses less energy, and ensures that the secondary phase is distributed uniformly due to a strong thermomechanical effect [39, 40], which improves the mechanical characteristics [41, 42]. In FSP, the material is manipulated at temperatures below its melting point and is only mechanically deformed in a plastic way. To create the composite, the reinforcing particles are mechanically combined with the plasticized metal. The fine dispersion of the reinforcement particles without segregation at the grain boundaries is the result of the base material not melting [43]. The pin geometry, the travel and rotational speeds, the tilt angle, and the number of FSP passes are only a few of the processing parameters that have an impact on the FSP process [44, 45].

The most common application of FSP is to modify the microstructure and mechanical properties of metallic components with thin surface layers [46–50]. Mehdi et al. [51] effective fabrication of an aluminum matrix composite (AMC) with nanoparticles of SiC and investigation of the microstructure and mechanical characteristics of the multi-pass FSP/SiC of AA6082-T6 The fabrication of the AZ91/SiC surface composite layers using the traditional FSP and friction stir vibration technique [52, 53]. The selection of reinforcing materials is primarily influenced by the targeted application and the compatibility of the particles with the substrate matrix. Boron carbide (B4C) is characterized by excellent neutron absorption as well as heat and wear resistance. Because of its high capacity for neutron absorption, B4C reinforced composites are used as the main neutron shield material in reactors [54]. Mg-CNT composites have exceptional mechanical properties, but Mg-Al2O3 composites have better wear resistance [55]. The hardness of the created composite was enhanced to 92% of the base metal in the carbon nanotubes/Mg alloy surface composite created using FSP [56]. The surface composite produced by adding Al2O3 reinforcement to an aluminium substrate demonstrated enhanced hardness when compared to the substrate material [57]. A 62% increase in hardness over matrix was stated for the Al7075/B4C surface composite [58].

Additionally, it was discovered that FSP composites significantly improved in microstructure changes, obtaining equiaxed and refined grain structures as opposed to the base metal's elongated and coarse grains, most likely as a result of the severe plastic deformation and continuous dynamic recrystallization brought on by FSP [59]. Friction stir processing (FSP) parameters were examined for their effects on the production of an AA6061/tungsten carbide nanocomposite. The results demonstrate that using the proper FSP settings results in an AA6061/WC nanocomposite free of voids and defects by uniformly dispersing the WC particles throughout the matrix [45, 60]. To experimentally explore surface generation and the best surface roughness to be achieved in relation to the process parameters, ultra-precision machining of particle reinforced metal matrix composites (MMCs) with polycrystalline diamond (PCD) end mill is carried out [61]. The dynamic cutting force modelling for precise micro milling of particle reinforced MMCs is the subject of a novel investigation presented [62].

Fiber reinforced metal matrix composites (MMCs) are a good option for applications in the automotive and aerospace industries and for military uses like defensive armors due to their mechanical characteristics. This study is an attempt to fabricate, characterize, and assess a metal matrix composite derived from this fascinating material, electrospun PAN, and EGNS/PAN nanofibers, using the FSP method. the analysis of the interfaces and subsequent mechanical characteristics of the metal matrix composites made by FSP, particularly the two PAN/AA5049 composites made from electrospun PAN nanofibers and exfoliated graphite nanosheets.

2 Experimental procedure

2.1 Materials

Polyacrylonitrile (PAN) with a molecular weight of 150,000 g/mol, catalogue no. (1813150), N, N-dimethylformamide (DMF purity 99.8%) was purchased from Aldrich catalogue no. (227056) and graphite flakes (GF, particle size 75 mesh, 99.9% min purity, catalogue number is 332461), were purchased from Sigma-Aldrich. Nitric acid and sulfuric acid were provided by Elnasr Pharmaceutical Chemicals Co., Egypt.

2.2 Electrospinning of EGNS/PAN/DMF

Our previous research [63] described the exfoliated graphite nanosheets (EGNS) fabrication process and procedures. First, sulfuric and nitric acid mixtures were mixed with graphite particles (ratio 4:1 by volume). The graphite intercalation compound was made by stirring the mixture constantly for 24 h at room temperature (GIC). The GIC was then cleaned with distilled water and dried to remove any moisture at 100 °C to produce expanded graphite, the dry particles were heated and thermally shocked for 30 s at 1050 °C. Finally, a 600-ml alcohol solution was poured over one gramme of expanded graphite (alcohol and distilled water with a ratio of 65:35). Before employing the dispersion in the electrospinning procedure, the dispersion was filtered and dried after 16 rounds of sonication to obtain the EGNS.

PAN/DMF polymer solution was prepared a ratio of 10 wt. % under continuous stirring at room temperature for 3 h to produce a homogeneous solution. EGNS were dispersed in DMF using ultrasonication for 16 h. The PAN/DMF polymer solution contained 10 weight percent of the EGNS weight concentration. The PAN was subsequently added to the EGNS/DMF suspension to produce a homogeneous and uniformly dispersed EGNS/PAN/DMF polymer solution. After that, the mixture was stirred for 10 h at 60 °C. The polymer solution was placed into a 10-mL glass syringe that was connected to a stainless-steel needle (inner diameter of 0.9 mm). A high voltage power supply was utilized to create a 25-kV electric field between the needle and a grounded, horizontally centered metal collector. The electrospun PAN and EGNS/PAN fibers were collected on a metal collector that was wrapped in aluminum foil. The collector was modified for all tests and placed 20 cm vertically from the needle tip for nanofiber deposition. Figure 1a shows the electrospinning technique.

2.3 Friction stir processing (FSP)

Aluminum (AA5049) sheet, whose chemical composition is shown in Table 1, was used to create surface composites. The base metal (BM) AA5049 sheets were wire-cut with dimensions of 100 × 50 × 6 mm. Applying wire electrical discharge machining, a rectangular groove with a depth and width of 3 mm and 1 mm, respectively, was created. The electrospun PAN nanofibers (or EGNS/PAN nanofibers) weighing 8 g were inserted into the wire-cut grooves.

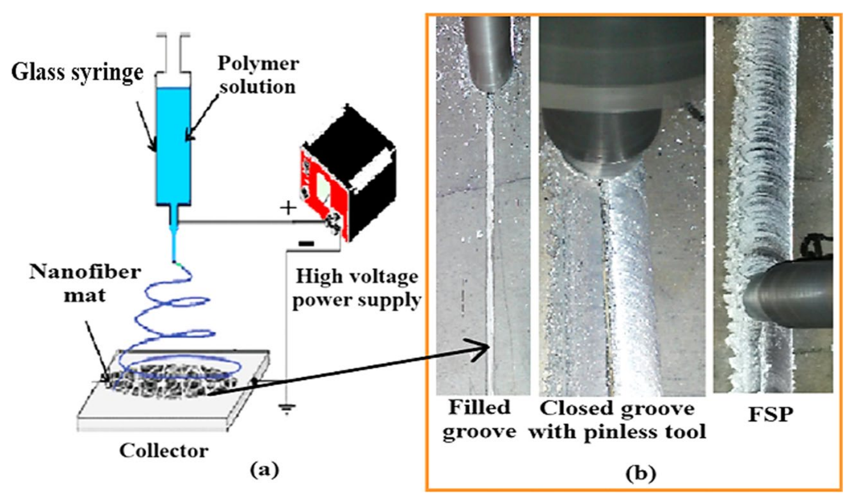

Fig. 1 **a** Electrospinning setup, **b** experimental procedure for fabricating nanofiber/AA5049 with FSP

Table 1 Chemical composition of aluminum AA5049

Element	Si	Fe	Cu	Mn	Mg	Cr	Ti	Al
Content (%)	0.17	0.35	0.08	0.8	1.9	0.12	0.05	balance

To prevent the escapement of any fabrics from the groove during processing, the groove entrance is initially sealed off using a tool with a shoulder without a pin. A computer numerical control vertical milling center with an FSP tool was used to produce the surface composite. The FSP tool had screwed pin profile, shoulder diameter of 18 mm, a pin diameter of 6 mm, and a height of 5.7 mm. Hardened H13 steel was used to manufacture the FSP tool. Based on the optimum values acquired from the prior study, the FSP process window was chosen [64]. The FSP tool rotation speed and traverse speed were both held constant at 1000 rpm and 40 mm/min, respectively. Figure 1b illustrates the FSP procedure.

3 Characterization

3.1 Scanning electron microscopy (SEM)

Scanning electron microscopy Model Quanta 250FEG (Field Emission Gun) with EDX Unit (energy dispersive X-ray analyses) at the Tabbin Institute for Metallurgical Studies (TIMS), Egypt was used to analyze the morphology of electrospun PAN,EGNS/PAN nanofiber and the distribution of the nanofiber reinforcement after FSP. The number of the points (about 100 random nanofibers) was correlated with the average diameter and distribution of the electrospun fibers. In each image, at the appropriate magnification, ImageJ software was used to measure the distance from the SEM. Microstructural samples were extracted from the AA5049 plates in the processed zone. Before displaying the surface metallographic, the surfaces of all samples were ground and polished to a mirror-like finish. Following mechanical polishing, the samples were etched with Keller's reagent (190 mL distilled water, 5 mL nitric acid, 3 mL hydrochloric acid, and 2 mL hydrofluoric acid). Also, the morphology of EGNS/PAN nanofiber was studied using a high-resolution transmission electron microscope (HRTEM) (JEOL model JEM 2100) at the Petroleum Research Institute in Egypt.

3.2 Mechanical characterization

A Vickers' microhardness tester was used to measure the microhardness at various points in the stir zone, with a 100-g load and 10-s dwell times. According to ASTM E8M-04 standards [65], the tensile sample is manufactured by wire cut EDM with dimensions of 2.5-mm-thick, 4-mm-wide, 58-mm-long, and a gauge length of 26 mm, as depicted in the Fig. 2. Uniaxial tensile tests are conducted with a cross-head speed of 1 mm/min at room temperature.

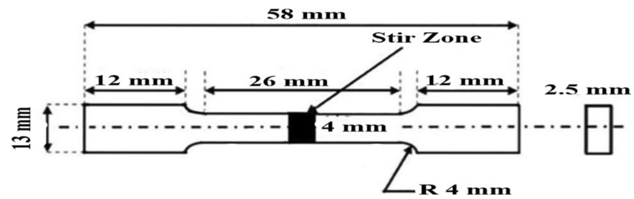

Fig. 2 Dimensions of the tensile test specimen

4 Results and discussion

4.1 Morphology of electrospun EGNS/PAN nanofiber composite

Figure 3a, b exhibit the morphology and diameter distribution of electrospun PAN nanofiber and EGNS/PAN composite nanofiber. As depicted in the figures, all of the fiber mats are uniformly distributed and randomly orientated. The electrospun PAN nanofibers have an average diameter of 195 ± 57 nm and a homogeneous, beadles morphology as shown in Fig. 3a. The morphology of EGNS/PAN electrospun nanofibers changed significantly after EGNS was incorporated. In a related nanocomposite, the diameter of electrospun nanofibers can be reduced by adding conductive nanofiller to the polymer matrix [66, 67]. Figure 3b shows EGNS/PAN nanofibers with decreased diameter after EGNS addition (180 ± 68 nm). The reduction in fiber diameter reveals that the electrical conductivity of EGNS can predominate in the decreasing of fiber diameter. Since graphene nanosheets have a large surface area, they exhibit powerful interactions with polymer matrices [68, 69]. The micrograph of EGNS/PAN composite nanofibers obtained by transmission electron microscopy (TEM) containing 10 weight percent EGNS is shown in Fig. 4. The EGNS layer on the PAN nanofiber surface is visible in the TEM image.

By using Raman spectroscopy, the presence of EGNS in the produced EGNS/PAN has been further established. The D-band line (1350 cm^{-1}) and the G-band line (1650 cm^{-1}) are two significant peaks in the Raman spectra of PAN/GO displayed in Fig. 5. The existence of these two bands strongly suggested that all composite nanofiber membranes have disordered and graphitic layers. The G bands on the EGNS/PAN nanofiber were noticeably higher than the D bands. The EGNS/PAN nanofiber with the I_D/I_G ratio of 0.95 suggested the presence of disordered graphite since the intensity ratio of the D band and G band is frequently utilized as an indicator for the degree of disorder [70, 71].

4.2 Microstructural characteristics

Optical micrographs of the FSP AA5049 substrate, PAN nanofiber, and EGNS/PAN nanofiber reinforced AA5049

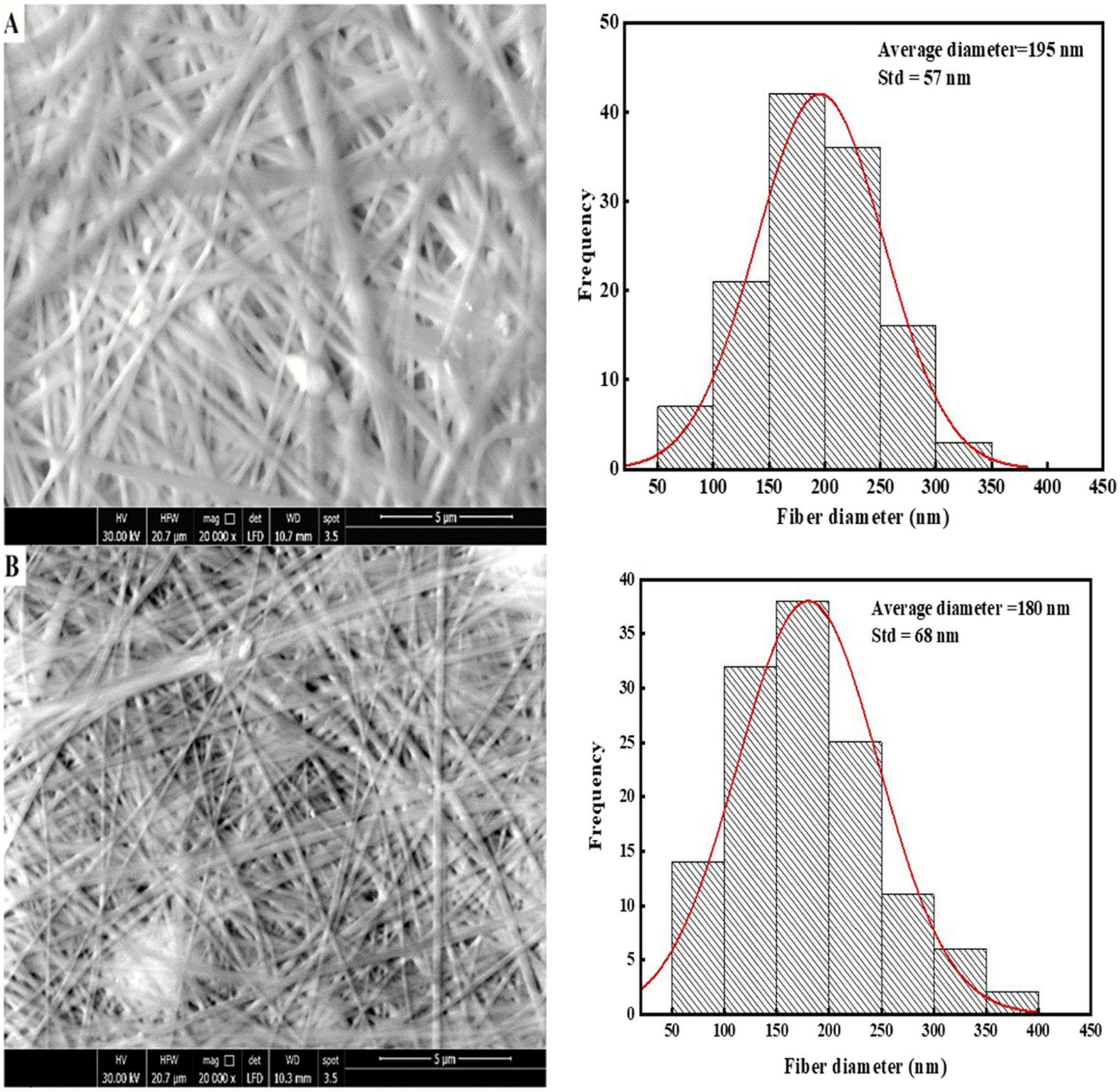

Fig. 3 Morphology and diameter distribution of electrospun: **a** PAN nanofiber; **b** EGNS/PAN nanofiber composite

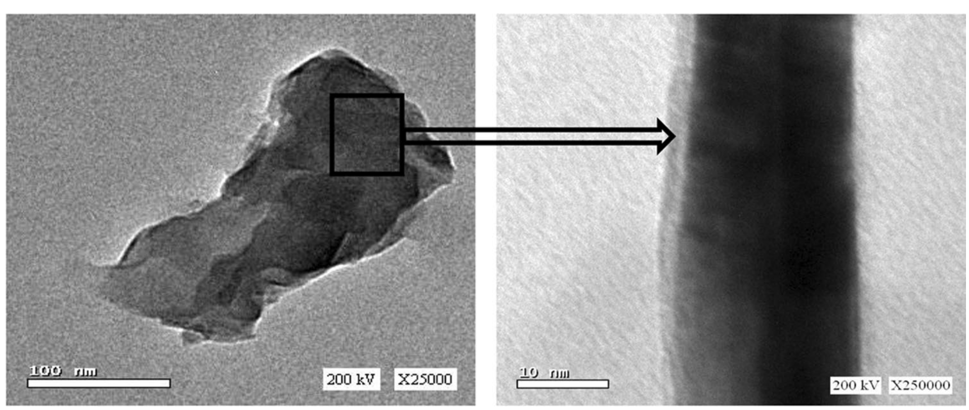

Fig. 4 TEM image of EGNS/PAN nanofiber composite

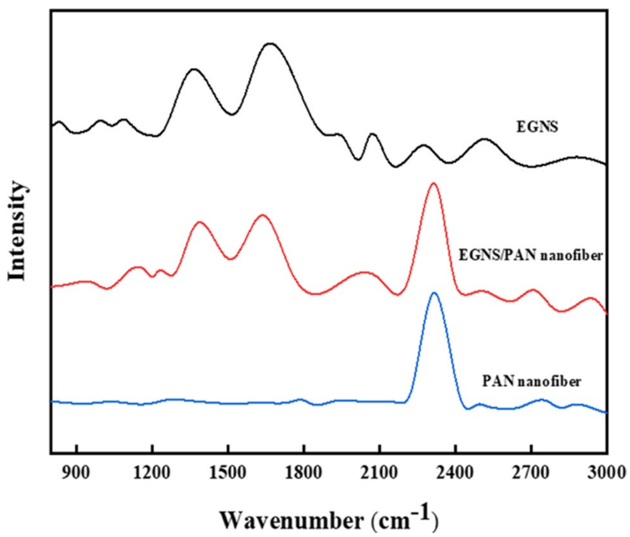

Fig. 5 Raman spectra of PAN, EGNS and EGNS/PAN nanofibers

taken at the stir zone are shown in Fig. 6a–c. A recrystallized fine-grained microstructure is produced within the stir zone as a result of the intense plastic deformation and frictional heating that occur during FSW and FSP. The term for this occurrence is dynamic recrystallization (DRX) [72, 73]. At the base of the stir zone, a concentric arc-shaped banded structure of PAN and EGNS/PAN nanofiber can be observed (Fig. 6b, c). This is an inherent feature of FSP and is termed as onion ring structure. An onion-ring structure is produced by the interaction of material flow between the warmer zone at the top and the colder zone at the bottom [74]. The rings of the tool tip during the FSP show that the distribution of Electrospun PAN Nano Fiber 195 ± 57 nm has been spread neatly inside the AA 5049 matrix (Fig. 6b). The presence of nanofibers caused onion rings to occasionally be rich and unreinforced. Regions with and without nanofibers are represented by the dark and light rings, respectively. Figure 6c shows that when particle-rich and particle-free regions were compared, the former had finer grains than the latter. It implies that in the FSP, strong plastic deformation separates the original grains and creates low angle, incorrectly oriented grain boundaries, leading to the growth of a significant number of nucleating zones for recrystallization. High-angle grain boundaries are created by DRX, which changes low-angle grain boundaries into finer grain patterns. Additionally, the “pinning effect” (Zener effect), which occurs when reinforcements are utilized in FSP, may cause these particles to block grain boundaries and stop grain coarsening by limiting their movement. Reinforcements, however, serve as nucleation zones and promote grain breakdown [72, 75, 76]. The grain structure refinement of the produced nanocomposite was accelerated by including EGNS/PAN nanofiber (180 ± 68 nm) inside the SZ. As a result of the additional dynamic recrystallization (DRX) in

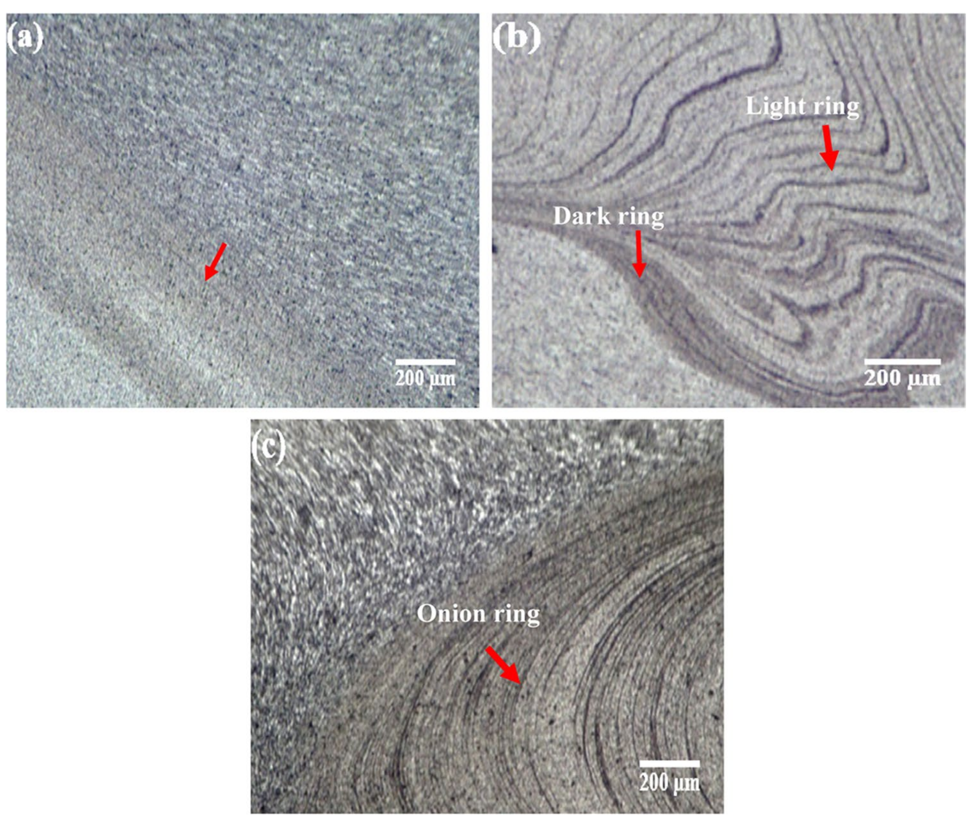

Fig. 6 Optical images displaying the microstructure of the stir zone of the FSP samples: **a** AA5049 substrate. **b** PAN nanofiber/AA 5049. **c** EGNS/PAN nanofiber/AA 5049

the stir zone, the matrix's grain size is reduced during FSP. It is anticipated that the inclusion of EGNS/PAN nanofibers will result in a more extensive microstructure refinement process when compared to the process using PAN nanofibers and without reinforcing. Figures 7 and 8 from the EDS analysis indicate the distribution of the different constituents in the PAN nanofiber and EGNS/PAN nanofiber reinforced AA 5049 surface composite. The EDS mapping analysis is applied to investigate the distribution of the reinforcements and the detrimental impacts of agglomeration and nanoclusters on the reinforcing nanofibers. In all samples, the reinforcing nanofibers were uniformly distributed in the SZ, and no significant clustering was observed. A typical EDS examination of an electrospun PAN, EGN/PAN nanofibers, the high aluminum concentration was identified, which was located at the boundary of the carbon nanofibers.

4.3 Mechanical results

4.3.1 Micro hardness behavior of MMNCs

Vickers micro-hardness curves for the AA5049 pure and SZ specimens as performed, with and without reinforcing nanofibers, are shown in Fig. 9. The average micro-hardness in the pure AA5049 and SZ is shown in Fig. 10. The pure AA 5049 has an average micro-hardness of 70 HV. The

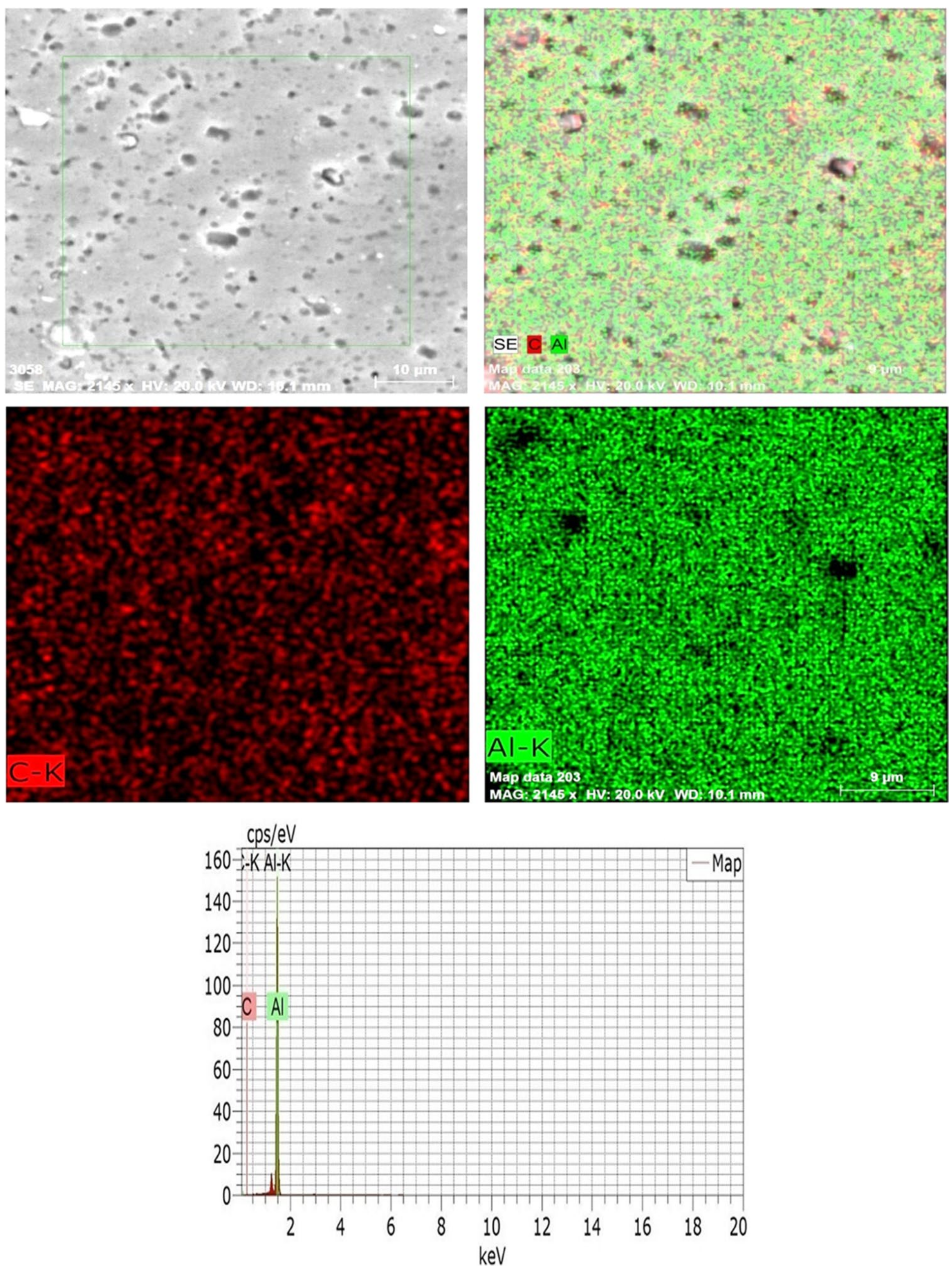

Fig. 7 EDS mapping evaluation in the SZ with PAN/AA 5049 reinforcement

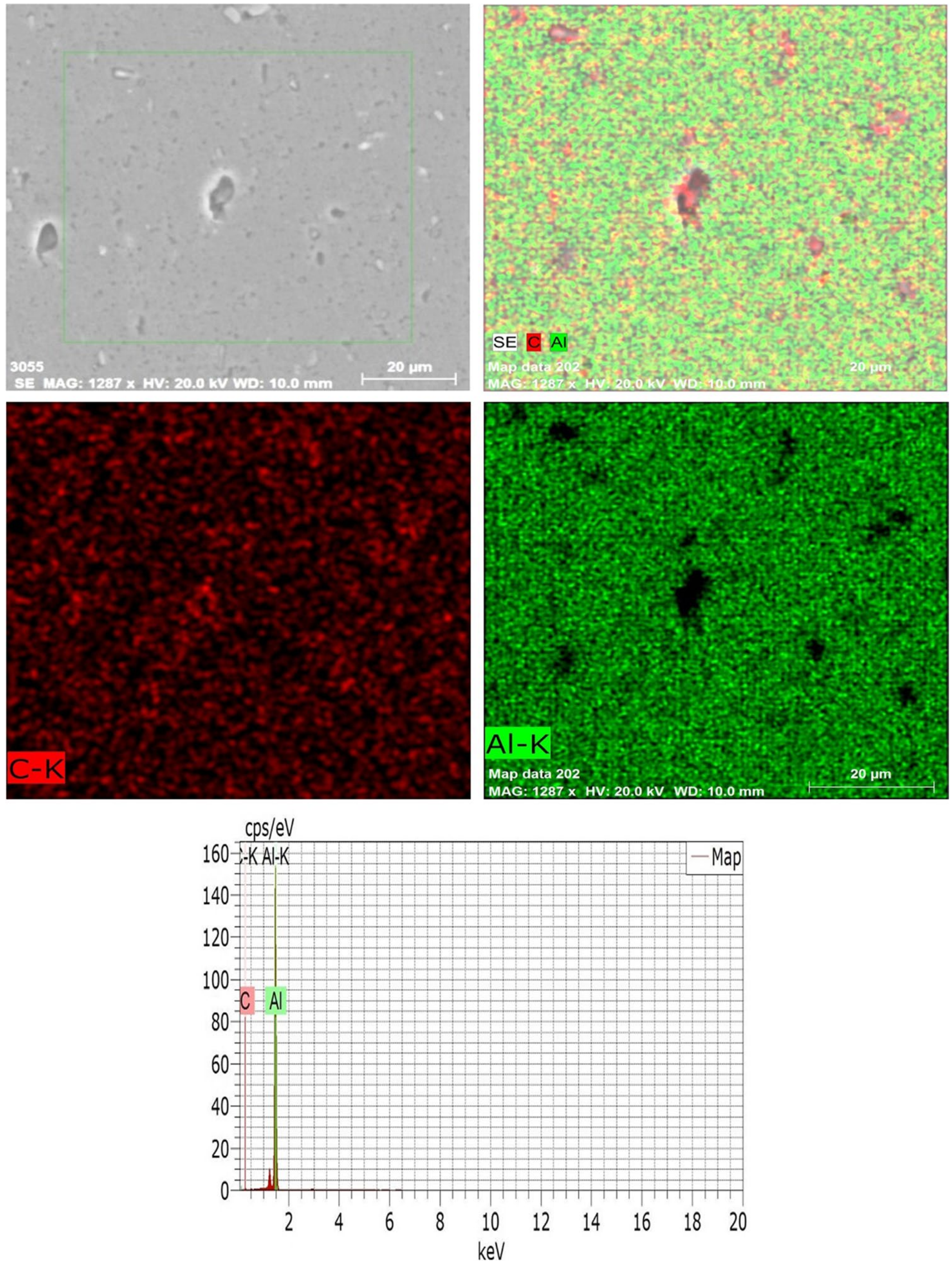

Fig. 8 EDS mapping evaluation in the SZ with EGNS/PAN/AA 5049 reinforcement

surface composite's SZ had increased hardness; the main factors contributing to this improvement were the uniform distribution and refining action of the nanofiber reinforcements. In the case of friction stir processed AA5049, the growth of fine grains and dislocations increased the initial hardness to 81 Hv. The hardness was increased to 89 and 98 Hv, respectively, by the reinforcement of PAN and EGNS/PAN nanofibers. The EGNS/PAN nanofiber has a harder reinforcement than pure AA5049, which results in a stronger reinforcement that strengthens the AA5049 matrix many folds [77]. The homogeneous distribution of electrospun EGNS/PAN nanofiber in the aluminum matrix enhances the strengthening since it serves as a barrier for the movement of dislocations. The variation in the thermal contraction coefficient of the matrix and the reinforcing phase is what causes the fine dispersion of the reinforcement nanofibers in addition to the quench hardening impact [78]. Additionally, compared to those produced by traditional FSP, the hardness values for weld zones under the inclusion of EGNS/PAN nanofibers are significantly greater. By enhancing localized stresses and hence the driving force for DRX, the inclusion of EGNS/PAN nanofibers results in better stored energy. When EGNS/PAN nanofibers are added during FSP, this inhibits grain growth by pinning the grain boundaries [79]. Therefore, the hardness of the electrospun nanofibers is transferred to the composite, further enhancing its hardness.

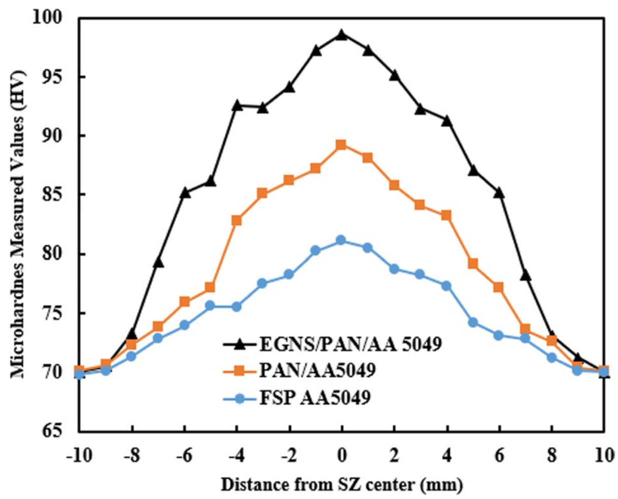

Fig. 9 Micro-hardness Profile for the investigated aluminum composites

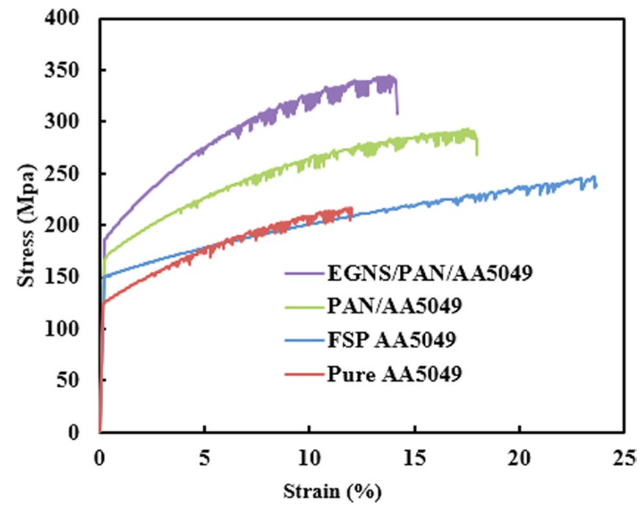

Fig. 11 Stress-strain curve for the investigated aluminum composites

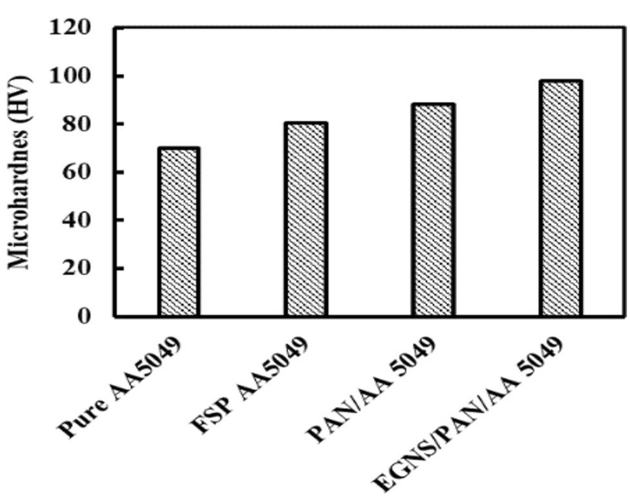

Fig. 10 Average micro-hardness values of pure AA5049 and the SZ for the investigated aluminum composites

4.3.2 Tensile properties

The stress-strain curves and tensile characteristics of the examined composites are shown in Fig. 11. Figure 12 indicates the mechanical properties of the investigated aluminum composites. The yield strength, ultimate strength, Young's modulus, and elongation to break of the pure AA5049 alloys were found to be 125 MPa, 216 MPa, 70 GPa, and 12%, respectively. During FSP, the processing region's microstructure was improved, which improved its mechanical and plastic properties and raised the elongation to break to 24%. The two main factors that had a substantial impact on the mechanical properties of the stirred zone material were dislocation strengthening and grain refining. The tensile performances were greatly increased by introducing particles because of the effects of particle uniformity, grain size refinement, and dislocation pinning [80, 81]. During FSP with nanofibers, the stir zone exhibits more severe plastic deformation and a larger dislocation density. Furthermore, it is well known that significant dislocation densities result from the temperature mismatch between the nanofibers and the matrix [82]. Despite the DRX phenomena taking place in the stir zone, the presence of nanofibers in the base matrix causes a high dislocation density around them. These dislocations may contribute to the tensile testing slip mechanism, resulting in a larger work-hardening capability. The pinning action of nanofibers prevents dislocations from migrating to grain boundaries, lowering the recovery rate [83, 84]. Additionally, it has been demonstrated that metal surface pre-treatment has a sizable impact on the mechanical performance of adhesively bonded joints. Metal surface pretreatment can increase the strength of the joints since one of the main bonding processes in FSP joints of the metal-composite is the adhesion forces caused by the presence of solidified molten polymer [85]. The ultimate tensile strength of the AA55049 increased to 291 and 344 MPa after being reinforced with PAN and EGNS/PAN nanofibers, with corresponding decreases in elongation (18 and 14.2%). This demonstrated the significant influence of nanofiber on alloy composites. For all composites, the yield strength and the elastic modulus were both improved. The electrospun nanofibers functioned as barriers for dislocation motions in the SZ, improving the mechanical characteristics of the produced composites. Improved mechanical characteristics were achieved as a result of the EGNS/PAN nanofiber's large specific surface area having good interfacial adhesion with the AA5049 matrix. Also, due to EGNS nanofillers' atomic thickness, excellent mechanical strength, and chemical inertness.

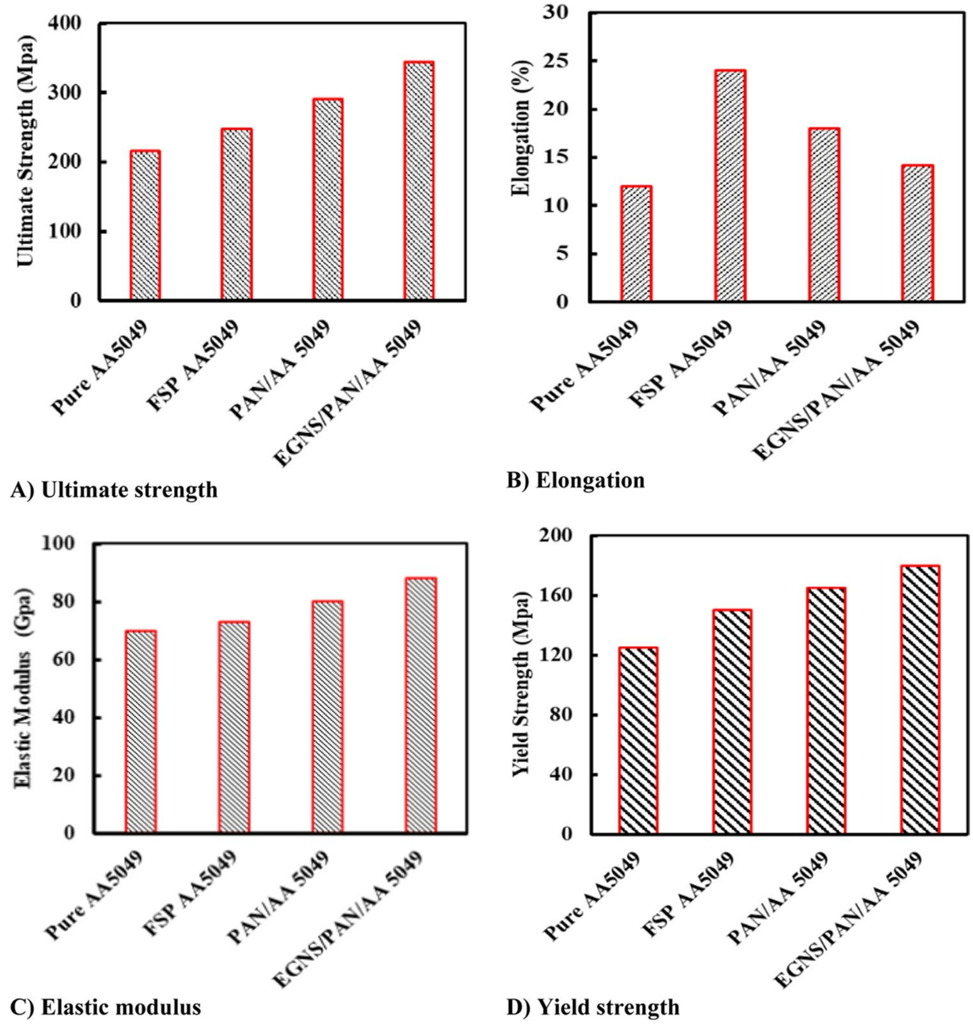

Fig. 12 Mechanical properties of the investigated aluminum composites

5 Conclusion

This work intends to describe the effects of the use of electrospun PAN and EGNS/PAN nanofibers during the FSP of aluminum 5049 to deal with a number of significant concerns, such as microstructure evolution, EDS, and mechanical characteristics. The findings indicate that:

1. The electrospun PAN diameter was found to be in the range of 195 ± 57 nm, whereas the electrospun EGNS/PAN nano fibril composite was reduced to 180 ± 68 nm by the presence of EGNS.
2. Microstructure analysis of composite samples revealed that both PAN and EGNS/PAN reinforcement were distributed uniformly inside the AA5049 metal matrix.
3. The FSP procedure results in the production of onion rings, and no voids or porosities with adequate diffusion are seen at the interface of the FSP with PAN and EGNS/PAN nanofibers.
4. EDS results showed The electrospun carbon nanofibers (C) cohesive with the predominant aluminum (AL) element.
5. The superior mechanical qualities of PAN and EGNS/PAN nanofibers, when introduced into the metal matrix, enhance the metal's strength, microhardness, and mechanical properties as a result to grain refinement, pinning effects, and dislocation density.
6. Microhardness was reported to be 89 and 98 Hv, respectively, for PAN and EGNS/PAN reinforcement, with a significant rise in microhardness along the SZ.
7. The tensile properties of the composites were apparently improved by 35% and 60%, respectively, by the incorporation of PAN and EGNS/PAN nanofibers.
8. The rising need for high-performance and lightweight materials in the aerospace and automotive industries as well as for military applications like defensive armor, the creation of metal matrix composites with PAN nanofibers and EGNS additives employing FSP has been gaining interest.

Acknowledgements No funding sources that supported the research presented.

Data availability Not applicable

Authors' contributions All authors have read and agreed to the research presented.

Funding Open access funding provided by The Science, Technology & Innovation Funding Authority (STDF) in cooperation with The Egyptian Knowledge Bank (EKB).

Declarations

Ethics approval and consent to participate Not applicable

Conflict of interest The authors declare that there is no conflict of interest.

References

1. Kuruvilla J, Oksman K, Gejo G, Wilson R, Appukuttan S (2021) Fiber reinforced composites: constituents, compatibility, perspectives and applications. Woodhead Publishing
2. Bahl S (2021) Fiber reinforced metal matrix composites-a review. Materials Today: Proceedings 39:317–323
3. Prashanth S, Subbaya KM, Nithin K, Sachhidananda S (2017) Fiber reinforced composites-a review. J Mater Sci Eng 6:2–6
4. Toloue EB, Karbasi S, Salehi H, Rafienia M (2019) Potential of an electrospun composite scaffold of poly (3-hydroxybutyrate)-chitosan/alumina nanowires in bone tissue engineering applications. Mater Sci Eng C 99:1075–1091
5. Cheng D, Li Y, Zhang J, Tian M, Wang B, He Z, Wang L (2020) Recent advances in electrospun carbon fiber electrode for vanadium redox flow battery: properties, structures, and perspectives. Carbon 170:527–542
6. Waldrop K, Wycisk R, Pintauro PN (2020) Application of electrospinning for the fabrication of proton-exchange membrane fuel cell electrodes. Current Opinion in Electrochemistry 21:257–264
7. Chen L, Chuang Y, Yang WD, Tsai KC, Chen CW, Dong CD (2021) All-inorganic perovskite CsPbX3 electrospun nanofibers with color-tunable photoluminescence and high performance optoelectronic applications. J Alloys Compd 856:157426
8. Zaca-Moran O, Sánchez-Ramírez JF, Herrera-Pérez JL, Díaz-Reyes J (2021) Electrospun polyacrylonitrile nanofibers as graphene oxide quantum dot precursors with improved photoluminescent properties. Mater Sci Semicond Process 127:105729
9. Al-Husaini IS, Lau WJ, RM YA, Al-Abri MZ, Al Farsi BA (2021) Synthesis of functional hydrophilic polyethersulfone-based electrospun nanofibrous membranes for water treatment. Journal of Environmental Chemical Engineering 9(1):104728
10. Norouzi M, Fazeli A, Tavakoli O (2020) Phenol contaminated water treatment by photocatalytic degradation on electrospun Ag/TiO2 nanofibers: Optimization by the response surface method. Journal of Water Process Engineering 37:101489
11. Beck RJ, Zhao Y, Fong H, Menkhaus TJ (2017) Electrospun lignin carbon nanofiber membranes with large pores for highly efficient adsorptive water treatment applications. Journal of water process engineering 16:240–248
12. Amariei G, Santiago-Morales J, Boltes K, Letón P, Iriepa I, Moraleda I, Rosal R (2017) Dendrimer-functionalized electrospun nanofibres as dual-action water treatment membranes. Sci Total Environ 601:732–740
13. Cui J, Li F, Wang Y, Zhang Q, Ma W, Huang C (2020) Electrospun nanofiber membranes for wastewater treatment applications. Sep Purif Technol 250:117116
14. Xu Z, Zhao H, Liang J, Wang Y, Li T, LuoY SX (2020) Noble-metal-free electrospun nanomaterials as electrocatalysts for oxygen reduction reaction. Materials Today Physics 15:100280
15. Mohraz MH, Yu IJ, Beitollahi A, Dehghan SF, Shin JH, Golbabaei F (2020) Assessment of the potential release of nanomaterials from electrospun nanofiber filter media. NanoImpact 19:100223
16. Han J, Xiong L, Jiang X, Yuan X, Zhao Y, Yang D (2019) Bio-functional electrospun nanomaterials: From topology design to biological applications. Prog Polym Sci 91:1–28
17. Da Silva BATT, Pascoalino LA, de Souza RL, Muniz EC, Curti PS (2020) Characterization of novel thermoresponsive poly (butylene adipate-co-terephthalate)/poly (N-isopropylacrylamide) electrospun fibers. Polym Bull 77:1157–1176
18. Suja PS, Reshmi CR, Sagitha P, Sujith A (2017) Electrospun nanofibrous membranes for water purification. Polym Rev 57:467–504
19. Kabir S, Medina S, Wang G, Bender G, Pylypenko S, Neyerlin KC (2020) Improving the bulk gas transport of Fe-NC platinum group metal-free nanofiber electrodes via electrospinning for fuel cell applications. Nano Energy 73:104791
20. Esfahani AR, Zhai L, Sadmani AA (2021) Removing heavy metals from landfill leachate using electrospun polyelectrolyte fiber mat-laminated ultrafiltration membrane. Journal of Environmental Chemical Engineering 9:105355
21. Al-Husaini IS, Yusoff ARM, Lau WJ, Ismail AF, Al-Abri MZ, Al-Ghafri BN, Wirzal MDH (2019) Fabrication of polyethersulfone electrospun nanofibrous membranes incorporated with hydrous manganese dioxide for enhanced ultrafiltration of oily solution. Sep Purif Technol 212:205–214
22. Awad R, Mamaghani AH, Boluk Y, Hashisho Z (2021) Synthesis and characterization of electrospun PAN-based activated carbon nanofibers reinforced with cellulose nanocrystals for adsorption of VOCs. Chem Eng J 410:128412
23. Cui J, Lu T, Li F, Wang Y, Lei J, Ma W, Huang C (2021) Flexible and transparent composite nanofibre membrane that was fabricated via a "green" electrospinning method for efficient particulate matter 2.5 capture. J Colloid Interface Sci 582:506–514
24. De Almeida DS, Martins LD, Muniz EC, Rudke AP, Squizzato R, Beal A, Gimenes ML (2020) Biodegradable CA/CPB electrospun nanofibers for efficient retention of airborne nanoparticles. Process Saf Environ Prot 144:177–185
25. Gao S, Liu Y, Jiang J, Li X, Ye F, Fu Y, Zhao L (2021) Thiram/hydroxypropyl-β-cyclodextrin inclusion complex electrospun nanofibers for a fast dissolving water-based drug delivery system. Colloids Surf B: Biointerfaces 201:111625
26. Kiadeh SZH, Ghaee A, Farokhi M, Nourmohammadi J, Bahi A, Ko FK (2021) Electrospun pectin/modified copper-based

metal–organic framework (MOF) nanofibers as a drug delivery system. Int J Biol Macromol 173:351–365
27. Guo Z, Tang G, Zhou Y, Shuwu L, Hou H, Chen Z, Huang C (2017) Fabrication of sustained-release CA-PU coaxial electrospun fiber membranes for plant grafting application. Carbohydr Polym 169:198–205
28. Thomas M, Rajiv S (2020) Grafted PEO polymeric ionic liquid nanocomposite electrospun membrane for efficient and stable dye sensitized solar cell. Electrochim Acta 341:136040
29. Dinesh VP, Sukhananazerin A, Sneha JM, Kumar PM, Biji P (2019) Novel stainless steel based, eco-friendly dye-sensitized solar cells using electrospun porous ZnO nanofibers. Nano-Structures - Nano-Objects 19:100311
30. Rosenberger AG, Dragunski DC, Muniz EC, Módenes AN, Alves HJ, Tarley CRT, Caetano J (2020) Electrospinning in the preparation of an electrochemical sensor based on carbon nanotubes. J Mol Liq 298:112068
31. Singh RK, Lye SW, Miao J (2021) Holistic investigation of the electrospinning parameters for high percentage of β-phase in PVDF nanofibers. Polymer 214:123366
32. Gupta A, Ayithapu P, Singhal R (2021) Study of the electric field distribution of various electrospinning geometries and its effect on the resultant nanofibers using finite element simulation. Chem Eng Sci 235:116463
33. Goyal A, Garg RK (2019) Establishing mathematical relationships to study tensile behavior of friction stir welded AA5086-H32 aluminium alloy joints. Silicon 11:51–65
34. Singh RK, Gilbert DR, Fitz-Gerald J, Lee DG (1997) Surface composites: novel method to fabricate adherent interfaces. Surf Eng 13:389–392
35. Zhao Y, Huang X, Li Q, Huang J, Yan K (2015) Effect of friction stir processing with B 4 C particles on the microstructure and mechanical properties of 6061 aluminum alloy. Int J Adv Manuf Technol 78:1437–1443
36. Berbon PB, Bingel WH, Mishra RS, Bampton CC, Mahoney MW (2001) Friction stir processing: a tool to homogenize nanocomposite aluminum alloys. Scr Mater 44:61–66
37. Ma ZY, Mishra RS, Mahoney MW, Grimes R (2005) Effect of friction stir processing on the kinetics of superplastic deformation in an Al-Mg-Zr alloy. Metall Mater Trans A 36:1447–1458
38. Manroo SA, Khan NZ, Ahmad B (2022) Development of nanocomposites on rare-earth Mg-ZE41 alloy via friction stir processing (FSP): microstructure, mechanical, and tribological properties. JOM 74:2047–2062
39. Huang Y, Wang T, Guo W, Wan L, Lv S (2014) Microstructure and surface mechanical property of AZ31 Mg/SiCp surface composite fabricated by direct friction stir processing. Mater Des 59:274–278
40. Abbasi M, Givi M, Bagheri B (2019) Application of vibration to enhance efficiency of friction stir processing. Trans Nonferrous Metals Soc China 29:1393–1400
41. Sunil BR, Reddy GPK, Patle H, Dumpala R (2016) Magnesium based surface metal matrix composites by friction stir processing. Journal of Magnesium and Alloys 4:52–61
42. Bagheri B, Abdollahzadeh A, Sharifi F, Abbasi M, Moghaddam AO (2021) Recent development in friction stir processing of aluminum alloys: microstructure evolution, mechanical properties, wear and corrosion behaviors. Proceedings of the Institution of Mechanical Engineers, Part E: Journal of Process Mechanical Engineering 09544089211058007
43. Dinaharan I, Zhang S, Chen G, Shi Q (2020) Development of titanium particulate reinforced AZ31 magnesium matrix composites via friction stir processing. J Alloys Compd 820:153071
44. Maboud AAGA, El-Mahallawy NA, Zoalfakar SH (2018) Process parameters optimization of friction stir processed Al 1050 aluminum alloy by response surface methodology (RSM). Materials Research Express 6:026527
45. Zoalfakar SH, Mohamed MA, Abdel Hamid M, Megahed AA (2022) Effect of friction stir processing parameters on producing AA6061/tungsten carbide nanocomposite. Proceedings of the Institution of Mechanical Engineers, Part E: Journal of Process Mechanical Engineering 236:653–667
46. Ma ZY (2008) Friction stir processing technology: a review. Metall Mater Trans A 39:642–658
47. Mehdi H, Mishra RS (2020) Effect of friction stir processing on microstructure and mechanical properties of TIG welded joint of AA6061 and AA7075. Metallography, Microstructure, and Analysis 9:403–418
48. Mehdi H, Mishra RS (2021) Effect of friction stir processing on mechanical properties and wear resistance of tungsten inert gas welded joint of dissimilar aluminum alloys. J Mater Eng Perform 30:1926–1937
49. Mehdi H, Mishra RS (2020) Influence of friction stir processing on weld temperature distribution and mechanical properties of TIG-welded joint of AA6061 and AA7075. Trans Indian Inst Metals 73:1773–1788
50. Chang CI, Du XH, Huang JC (2007) Achieving ultrafine grain size in Mg–Al–Zn alloy by friction stir processing. Scr Mater 57:209–212
51. Mehdi H, Mishra RS (2021) Effect of multi-pass friction stir processing and SiC nanoparticles on microstructure and mechanical properties of AA6082-T6. Advances in Industrial and Manufacturing Engineering 3:100062
52. Abdollahzadeh A, Bagheri B, Abbasi M, Sharifi F, Moghaddam AO (2021) Mechanical, wear and corrosion behaviors of AZ91/SiC composite layer fabricated by friction stir vibration processing. Surface Topography: Metrology and Properties 9:035038
53. Bagheri B, Abbasi M, Abdollahzadeh A, Mirsalehi SE (2020) Effect of second-phase particle size and presence of vibration on AZ91/SiC surface composite layer produced by FSP. Trans Nonferrous Metals Soc China 30:905–916
54. Abdelhady SS, Elbadawi RE, Zoalfakar SH (2023) Investigation of the microstructure, mechanical and wear performance of friction stir-processed AA6061-T6 plate reinforced with B4C particles surface composite. J Compos Mater 00219983231171286
55. Wang W, Shi QY, Liu P, Li HK, Li T (2009) A novel way to produce bulk sicp reinforced aluminium metal matrix composites by friction stir processing. J Mater Process Technol 209:2099–2103
56. Arab SM, Zebarjad SM, Ahmad S, Jahromi J (2017) Fabrication of AZ31/MWCNTs Surface metal matrix composites by friction stir processing: investigation of microstructure and mechanical properties. J Mater Eng Perform 26:5366–5374
57. Mobasherpour I, Tofigh AA, Ebrahimi M (2013) Effect of nano-size Al2O3 reinforcement on the mechanical behavior of synthesis 7075 aluminum alloy composites by mechanical alloying. Mater Chem Phys 138:535–541
58. Ramesh R, Murugan N (2012) Production and characterization of aluminium 7075–T651 Alloy/B4C surface composite by friction stir processing. Int J Eng Adv Technol 1:88–90
59. El-Mahallawy NA, Zoalfakar SH, Maboud AA (2019) Microstructure investigation, mechanical properties and wear behavior of Al 1050/SiC composites fabricated by friction stir processing (FSP). Materials Research Express 6(9):096522
60. Megahed AA, Mohamed MA, Abdel Hamid M, Zoalfakar SH (2022) Microstructure, hardness, and wear properties of AA6061/WC nanocomposite fabricated by friction stir processing. Proc Inst Mech Eng C J Mech Eng Sci 236:9148–9156
61. Niu Z, Cheng K (2019) An experimental investigation on surface generation in ultraprecision machining of particle reinforced metal matrix composites. Int J Adv Manuf Technol 105:4499–4507

62. Niu Z, Cheng K (2020) Improved dynamic cutting force modelling in micro milling of metal matrix composite's part II: Experimental validation and prediction. Proc Inst Mech Eng C J Mech Eng Sci 234:1500–1515
63. Abdelhady SS, Elbadawi RE, Zoalfakar SH (2022) Fabrication of electrospun exfoliated graphite nanosheets/polystyrene composite nanofiber mats. J Thermoplast Compos Mater:1–17
64. Sathiskumar R, Murugan N, Dinaharan I, Vijay SJ (2014) Prediction of mechanical and wear properties of copper surface composites fabricated using friction stir processing. Mater 55:224–234
65. ASTM-E8M (2016) Standard test methods for tension testing of metallic material. In: Annual book of ASTM standards. American Society for Testing and Materials, West Conshohocken
66. Bahrami S, Solouk A, Mirzadeh H, Seifalian AM (2019) Electroconductive polyurethane/ graphene nanocomposite for biomedical applications. Compos B Eng 168:421–431
67. Tijing LD, Park C-H, Choi WL, Ruelo MTG, Amarjargal A, Pant HR, Kim CS (2013) Characterization and mechanical performance comparison of multiwalled carbon nanotube/polyurethane composites fabricated by electrospinning and solution casting. Compos B Eng 44:613–619
68. Yu W, Zhang X, Gao X, Liu H, Zhang X (2020) Fabrication of high-strength PET fibers modified with graphene oxide of varying lateral size. J Mater Sci 55:8940–8953
69. Jia Y, Chen L, Yu H, Zhang Y, Dong F (2015) Graphene oxide/ polystyrene composite nanofibers on quartz crystal microbalance electrode for the ammonia detection. RSC Adv 5:40620–40627
70. Sahu RS, Bindumadhavan K, Doong R (2017) Boron-doped reduced graphene oxide-based bimetallic Ni/Fe nanohybrids for the rapid dechlorination of trichloroethylene. Environ Sci: Nano 4:565–576
71. Muzyka R, Drewniak S, Pustelny T, Chrubasik M, Gryglewicz G (2018) Characterization of graphite oxide and reduced graphene oxide obtained from different graphite precursors and oxidized by different methods using Ramanspectroscopy. Materials 11:1050
72. Sun YF, Fujii H (2011) The effect of SiC particles on the microstructure and mechanical properties of friction stir welded pure copper joints. Mater Sci Eng A 528:5470–5475
73. Bahrami M, Dehghani K, Besharati Givi MK (2014) A novel approach to develop aluminum matrix nano-composite employing friction stir welding technique. J Mater Des 53:217–225
74. Morisada Y, Fujii H, Nagaoka T, Nogi K, Fukusumi M (2007) Fullerene/A5083 composites fabricated by material flow during friction stir processing. Composites Part A 38:2097–2101
75. Bagheri B, Shamsipur A, Abdollah Zadeh A, Mirsalehi SE (2023) Investigation of SiC nanoparticle size and distribution effects on microstructure and mechanical properties of Al/SiC/Cu composite during the FSSW process: experimental and simulation. Met Mater Int 29:1095–1112
76. Rizi VS, Abbasi M, Bagheri B (2021) Investigation into microstructure and mechanical behaviors of joints made by friction stir vibration brazing between low carbon steels. Phys Scr 96:125704
77. Zhang Z, Chen DL (2006) Consideration of Orowan strengthening effect in particulatereinforced metal matrix nanocomposites: a model for predicting their yield strength. Scr Mater 54:1321–1326
78. Selvaraju S, Senthamaraikannan S, Jayaprakasham S, Madiq AR (2018) Effect of process parameters on microstructure and mechanical properties of friction stir welded cast nickel aluminum bronze alloy (C95800). Mater Res 21:0603
79. Bagheri B, Alizadeh M, Mirsalehi SE, Shamsipur A, Abdollahzadeh A (2022) Nanoparticles addition in AA2024 aluminum/pure copper plate: FSSW approach, microstructure evolution, texture study, and mechanical properties. Jom 74:4420–4433
80. Ma K, Wen H, Hu T, Topping TD, Isheim D, Seidman DN, Schoenung JM (2014) Mechanical behavior and strengthening mechanisms in ultrafine grain precipitation-strengthened aluminum alloy. Acta Mater 62:141–155
81. Abdollahzadeh A, Bagheri B, Shamsipur A (2022) Development of Al/Cu/SiC bimetallic nano-composite by friction stir spot welding. Mater Manuf Process:1–10
82. Bagheri B, Abbasi M (2020) Development of AZ91/SiC surface composite by FSP: Effect of vibration and process parameters on microstructure and mechanical characteristics. Adv Manuf 8:82–96
83. Khorrami MS, Saito N, Miyashita Y, Kondo M (2019) Texture variations and mechanical properties of aluminum during severe plastic deformation and friction stir processing with SiC nanoparticles. Mater Sci Eng A 744:349–364
84. Zhang L, Chandrasekar R, Howe JY, West MK, Hedin NE, Arbegast WJ, Fong H (2009) A metal matrix composite prepared from electrospun TiO2 nanofibers and an Al 1100 alloy via friction stir processing. ACS Appl Mater Interfaces 1:987–991
85. André NM, Goushegir SM, dos Santos JF, Canto LB, Amancio-Filho ST (2018) Influence of the interlayer film thickness on the mechanical performance of AA2024-T3/CF-PPS hybrid joints produced by friction spot joining. Weld Int 32:1–1